Journal of Sound and Vibration (2000) **234**(2), 225–239
doi:10.1006/jsvi.1999.2875, available online at http://www.idealibrary.com on IDEAL®

AN INVESTIGATION INTO INTEGRAL EQUATION METHODS INVOLVING NEARLY SINGULAR KERNELS FOR ACOUSTIC SCATTERING

S. A. YANG

Department of Naval Architecture and Marine Engineering, National Cheng Kung University, Tainan, Taiwan, Republic of China

(*Received* 21 *June* 1999, *and in final form* 17 *November* 1999)

This work presents a numerical means of investigating the acoustic scattering by disk-shaped bodies. On the basis of Burton and Miller's method, the singularity-free formulations of Helmholtz integral equation and its normal derivative are used to form a composite equation. A triangle polar co-ordinate transformation method is further applied to treat the nearly singular kernels arising from a situation in which the field points and source points are very close together. Numerical simulations consist of the acoustic scattering by a short circular cylinder and a thin circular disk respectively. For the latter case with zero thickness, the corresponding analytical solutions involving angular and radial oblate spheroidal wave functions are evaluated as well. Comparing the numerical results with the experimental data and analytical solutions demonstrates the effectiveness of the proposed method.

1. INTRODUCTION

Integral equation (IE) methods are a conventional means of treating many physical problems, including acoustics, fluid mechanics, steady state heat conduction, elastostatics, magnetostatics, and fracture mechanics. When the working domain extends to infinity, IE methods are highly attractive in that the problem's dimensionality is reduced by one, and the infinite domain is transformed to finite boundaries in which the farfield condition is automatically satisfied, provided that an appropriate Green's function is applied. Regarding acoustic scattering and radiation, two conventional methods based on the IE approach have been proposed to avert the well-known non-uniqueness problem. The first method, combined Helmholtz integral equation formulation (CHIEF), was proposed by Schenck [1]. The second method, composite outward normal derivative overlap relation (CONDOR), was advocated by Burton and Miller [2] which linearly combines the Helmholtz integral equation with its normal derivative. Both methods have their own limitations even for smooth body shapes, accounting for why numerous investigations have ttempted to enhance the numerical reliability, efficiency, and accuracy [3]. See also a recent paper by Benthien and Schenck [4] for a brief review of various methods.

Moreover, for disk-shaped bodies and bodies with sharp edges or corners, nearly singular integrals appear in the IE formulation. Accurately assessing such integrals is generally much more difficult than the weakly singular and Cauchy principal value singular integrals [5]. Under such circumstances, two conventional approaches can be applied to yield accurate results. The sub-division method increases the number of sub-divisions and the

0022-460X/00/270225 + 15 $35.00/0

adaptive quadrature method increases the order of the quadrature formula around the nearly singular point [6]. Such approaches, however, are expensive in computation and pose a difficulty in globally controlling accuracy. For the potential problems, other alternative approaches have been proposed to avert this difficulty [7]. For instance, applying appropriate transformations can map domains with corners onto domains with smooth boundaries. Another approach expresses the harmonic function in the form of an infinite series in the neighborhood of a corner [8, 9]. Heise [10] further demonstrated that if a fundamental solution on a Riemann surface with an optimal number of sheets is chosen, several kernels in integral equations vanish on the flanks of a sector. Consequently, a potential problem on a domain with a corner can be formulated as an integral equation taken over a part of the boundary, which does not contain the neighborhood of the corner. Sladek *et al.* [11] also proposed a superposition principal method for the regularization. We refer the reader to references [12–14] for the more detailed discussions. Although above-mentioned approaches have not been extended to the acoustical problems, research involving the nearly singular singularity has been a main theme of the potential and other problems. The reasons may be ascribed to the fact that the CHIEF and CONDOR methods are already complicated in terms of formulation and the normal vector at a corner cannot be defined. Therefore, other efficient methods deemed appropriate for the current acoustical problem are highly desired.

For thin-body scattering, every field point on the boundary possesses both singularity and near singularity in the IE formulation, thereby complicating numerical implementation. The so-called multidomain boundary element formulation is an effective means of averting such a difficulty when the disk-shaped body's thickness degenerates [15, 16]. However, such an approach fails to simulate a disk-shaped body with a noticeable thickness since the continuity condition of the normal velocity across a body with zero thickness cannot be applied. Krishnasamy *et al.* [17] applied the CONDOR approach to eliminate the fictitious eigenfrequencies. The nearly singular integrals were evaluated by the use of Taylor's expansion, Stokes' theorem, a polar co-ordinate transformation and other specific treatments. In light of the above developments, this paper presents an effective means of simultaneously evaluating the singular and nearly singular integrals such that the acoustic scattering by disk-shaped bodies and bodies with edges or corners can be studied without numerical difficulty. The rest of this paper is organized as follows. Section 2 outlines the fundamental equations of the problem. On the basis of Burton and Miller's method, the composite integral equation in a completely singularity-free form derived by Hwang [18] is used. In contrast to other regularization schemes, this formulation globally regularizes weak and hypersingular kernels and, therefore, can be directly implemented using standard quadrature formulae. On the other hand, Huang and Cruse [5] developed a novel scheme to efficiently evaluate the nearly singular integrals by applying two successive co-ordinate transformations. Other investigations further developed a generalization of Huang and Cruse's method by replacing one of the transformations with a triangle polar co-ordinate transformation [19, 20]. Section 3 describes this method with an appropriate modification suitable for the current problem. Some preliminary test examples are presented as well. Combining formulations in Sections 2 and 3 yields the solution method for the current problem. Section 4 examines the proposed method's effectiveness by solving the acoustic scattering from a rigid circular cylinder with length $2h$ and radius a. The edge effect is examined by assigning $h/a = 1$ and the dimensionless wave number ka varying from one to seven. The second example investigates the thickness effect by assigning $h/a = 0{\cdot}0423$, $0{\cdot}02$ and, again, ka varying from one to seven. Comparisons are made with the experimental data and analytical solutions. Conclusions are finally made in section 5.

2. INTEGRAL EQUATION FORMULATION

The propagation of acoustic waves through an unbounded homogeneous medium is described by the wave equation

$$\nabla^2 \phi(r, t) = \frac{1}{c^2} \frac{\partial^2 \phi(r, t)}{\partial r^2}, \tag{1}$$

where ∇^2 denotes the Laplacian operator, ϕ the velocity potential at a point r at time t, and c the speed of sound in the medium at the equilibrium state. The velocity potential can be written by summing the two parts as follows:

$$\phi = \phi^i + \phi^s, \tag{2}$$

where ϕ^i denotes the incident velocity potential and ϕ^s represents the scattered velocity potential. For a steady state excitation with a time factor $\exp(-\mathrm{i}\omega t)$, equation (1) reduces to the Helmholtz differential equation in the following form:

$$(\nabla^2 + k^2)\phi = 0, \tag{3}$$

where i denotes the imaginary unit, ω the angular frequency, and $k = \omega/c$ the wave number. The excess acoustic pressure can be written as

$$p = \mathrm{i}\omega\rho_0 \phi, \tag{4}$$

where ρ_0 denotes the density of the fluid at the equilibrium state. The scattered velocity potential should also satisfy the Sommerfeld radiation condition, which can be written in a three-dimensional form as

$$\lim_{r \to \infty} r \left| \frac{\partial \phi^s}{\partial r} - \mathrm{i}k\phi^s \right| = 0. \tag{5}$$

The corresponding integral formulation of equation (3) can be written as follows:

$$\varepsilon\phi(P) = \phi^i(P) + \int_S \left(\phi(Q) \frac{\partial G_k(P, Q)}{\partial n_Q} - G_k(P, Q) \frac{\partial \phi(Q)}{\partial n_Q} \right) \mathrm{d}S_Q, \tag{6}$$

where n_Q denotes the distance in the direction of the outward normal at the source point Q and S represents the body surface. The free-space Green's function in a three-dimensional form can be expressed as

$$G_k(P, Q) = \mathrm{e}^{\mathrm{i}kR}/4\pi R, \tag{7}$$

where R denotes the distance between the field point $P(x, y, z)$ and the source point $Q(\xi, \eta, \zeta)$. The value of factor ε depends on the position of P, i.e.,

$$\varepsilon = \begin{cases} 1 & \text{for } P \in S_e, \\ \frac{1}{2} & \text{for } P \in \text{smooth } S, \\ 0 & \text{for } P \in S_i, \end{cases} \tag{8}$$

where S_e denotes the infinite domain exterior to S, and S_i represents the interior domain enclosed by S. For P on the surface with a sharp corner, ε is related to the solid angle Ω by

$$\begin{aligned}\varepsilon &= 1 - \Omega/4\pi \\ &= 1 + \frac{1}{4\pi}\int_S \frac{\partial}{\partial n_Q}\left(\frac{1}{R}\right) \mathrm{d}S_Q. \end{aligned} \tag{9}$$

The boundary relation of equation (6) fails to yield unique solutions at certain characteristic frequencies. Non-uniqueness is a purely mathematical problem arising from the breakdown of boundary integral representation rather than from the nature of the physical problem. To avert this difficulty, a second equation can be obtained by differentiating equation (6) in the normal direction at P:

$$\varepsilon \frac{\partial \phi}{\partial n_P} = \frac{\partial \phi^i}{\partial n_P} + \frac{\partial}{\partial n_P}\int_S \phi(Q) \frac{\partial G_k(P, Q)}{\partial n_Q} \mathrm{d}S_Q - \int_S \frac{\partial G_k(P, Q)}{\partial n_P} \frac{\partial \phi}{\partial n_Q} \mathrm{d}S_Q. \tag{10}$$

Linearly combining equation (6) with equation (10) allows us to obtain unique solutions for all real frequencies when the coupling parameter is selected such that its imaginary part is non-zero [2]. Notably, the need to evaluate the hypersingular integral in equation (10) largely hinders the numerical implementation of the composite equation. Numerous investigations have attempted to efficiently evaluate the hypersingular integral. Most of the schemes alleviate the highly singular behavior only, and leave a weak singularity in the final formulation. The weak singularity is then locally regularized using a co-ordinate transformation. In contrast, Hwang's formulation was derived using a global approach [18]. Herein, we adopt this formulation owing to its accuracy and efficiency in computation. See also Yang [21] for a more detailed discussion of this approach.

By considering a Neumann boundary condition, $\partial\phi/\partial n = 0$, and assigning $\varepsilon = \frac{1}{2}$, equation (6) reduces to

$$\frac{\phi(P)}{2} = \phi^i(P) + \int_S \phi(Q) \frac{\partial G_k(P, Q)}{\partial n_Q} \mathrm{d}S_Q \tag{11}$$

in which $\partial G_k/\partial n$ is weakly singular [9]. Equation (11) can be expressed in a regular form as follows:

$$\phi(P) = \phi^i(P) + \int_S \left[\phi(Q) \frac{\partial G_k}{\partial n_Q} - \phi(P) \frac{\partial G_0}{\partial n_Q}\right] \mathrm{d}S_Q, \tag{12}$$

where $G_0 = \frac{1}{4}\pi R$ denotes the free-space Green's function for Laplace equation. The integrand in equation (12) is set equal to zero when Q coincides with P. Under the same boundary condition, equation (10) reduces to

$$\frac{\partial \phi^i}{\partial n_P} = -\frac{\partial}{\partial n_P}\int_S \phi(Q) \frac{\partial G_k(P, Q)}{\partial n_Q} \mathrm{d}S_Q. \tag{13}$$

The preceding equation can be rewritten as follows:

$$\frac{\partial \phi^i}{\partial n_P} = -\int_S \phi(Q) \frac{\partial^2 (G_k - G_0)}{\partial n_P \partial n_Q} \mathrm{d}S_Q - \int_S \frac{\partial G_0}{\partial n_P} \frac{\partial \varphi}{\partial n_Q} \mathrm{d}S_Q + \frac{1}{2}\frac{\partial \varphi}{\partial n_P}, \tag{14}$$

where φ is a velocity potential of Laplace equation. Notably, the hypersingular integral in equation (13) is converted into two weakly singular integrals plus a function $\partial\varphi/\partial n$ in equation (14). Furthermore, equation (14) can be expressed in a regular form as follows:

$$\frac{k^2\Phi_e}{2\sigma(P)}\phi(P) = \frac{\partial\phi^i}{\partial n_P} - \frac{\partial\varphi}{\partial n_P} + \int_S \left[\phi(Q)\frac{\partial^2(G_k - G_0)}{\partial n_P \partial n_Q} - \frac{k^2 G_0 \sigma(Q)}{2\sigma(P)}\phi(P)\right] + \int_S \left[\frac{\partial G_0}{\partial n_P}\frac{\partial\varphi}{\partial n_Q} - \frac{\partial G_0}{\partial n_Q}\frac{\partial\varphi}{\partial n_P}\right] \mathrm{d}S_Q, \tag{15}$$

where the first and second integrands are set equal to $\mathrm{i}k^3\phi(P)/12\pi$ and zero, respectively, when Q coincides with P. Notably, equation (15) introduces three extra unknowns, i.e., σ, Φ_e and $\partial\varphi/\partial n$. Herein, the surface source function σ makes the surface potential an equipotential Φ_e, which is defined by

$$\Phi_e = -\int_S \sigma(Q) G_0 \,\mathrm{d}S_Q. \tag{16}$$

The preceding equation contains a weakly singular integral. However, the fact that Φ_e remains constant in the interior of an equipotential surface accounts for why its value can be conveniently computed by locating point P inside the boundary surface. For instance, locating the origin of the co-ordinate system inside the boundary surface and, furthermore, locating the field point P at the origin yields

$$\Phi_e = -\frac{1}{4\pi}\int_S \frac{\sigma(Q)}{(\xi^2 + \eta^2 + \zeta^2)^{1/2}}\,\mathrm{d}S_Q. \tag{17}$$

Herein, the function σ can be expressed as

$$\sigma(P) = -2\int_S \sigma(Q)\frac{\partial G_0}{\partial n_P}\,\mathrm{d}S_Q. \tag{18}$$

This equation can be rewritten in a regular form as

$$0 = \int_S \left[\sigma(Q)\frac{\partial G_{0\cdot}}{\partial n_P} - \sigma(P)\frac{\partial G_0}{\partial n_Q}\right]\mathrm{d}S_Q, \tag{19}$$

where the integrand is set equal to zero when Q coincides with P. The function $\partial\varphi/\partial n$ is determined by

$$\frac{\Phi_e}{\sigma(P)}\frac{\partial\varphi}{\partial n_P} = \int_S G_0\left[\frac{\partial\varphi}{\partial n_Q} - \frac{\sigma(Q)}{\sigma(P)}\frac{\partial\varphi}{\partial n_P}\right]\mathrm{d}S_Q - \int_S [\phi(Q) - \phi(P)]\frac{\partial G_0}{\partial n_Q}\,\mathrm{d}S_Q, \tag{20}$$

where both the integrands are set equal to zero when Q coincides with P.

In the numerical implementation, the functions σ and Φ_e are evaluated in advance, and then ϕ and $\partial\varphi/\partial n$ are simultaneously solved. Following the regularization scheme in a manner similar to Hwang, Yang [21] derived a two-dimensional variant of the singularity-free formulations subject to Neumann and Dirichlet conditions respectively. That investigation also compared the efficiency of Yang's and Hwang's formulations with the formulations proposed by others. Moreover, Yang [22] successfully extended the formulations presented above to investigate acoustic scattering from perfectly hard and soft bodies across a wide frequency range.

3. A METHOD OF EVALUATING NEARLY SINGULAR INTEGRALS

In the previous section, the weak and hypersingular kernels were desingularized using some properties of potential theory. The formulations can be implemented without difficulty in most engineering applications with one exception, when the nearly singular kernels appear. The nearly singular kernels appear when the field points and source points are extremely close together. This section describes an efficient means of evaluating nearly singular integrals [5, 19, 20].

Let us consider an integral in the following form:

$$I = \int\int \frac{g}{R^n} \, d\gamma \, d\lambda, \tag{21}$$

where g denotes a function and n represents an integer. Herein, efficiently evaluating I for a small value of R is of primary concern. Allow $R_0 = R(\gamma_0, \lambda_0)$ to be a distance from the field point to the point on the integration domain that is closest to the field point. Equation (21) can be rewritten as

$$I = \int\int \frac{g}{[(R - R_0) + R_0]^n} \, d\gamma \, d\lambda = \int\int \frac{g}{[(R - R_0) + R_0]^n} \, du \, dv, \tag{22}$$

where the (u, v) co-ordinates are defined by $u = \gamma - \gamma_0$ and $v = \lambda - \lambda_0$. The triangle polar co-ordinate transformation method divides the integration domain into several triangles around the point $(u, v) = (0, 0)$, which is referred to as the first vertex of the triangles. The second and third vertices of a triangle, counted counterclockwise, are denoted by $(u^{(2)}, v^{(2)})$ and $(u^{(3)}, v^{(3)})$ respectively. The relationships

$$u = \mu(1 - \beta)u^{(2)} + \mu\beta u^{(3)}, \qquad v = \mu(1 - \beta)v^{(2)} + \mu\beta v^{(3)} \tag{23}$$

map each triangle into a unit square in the (μ, β) co-ordinates. Correspondingly, the Jacobian can be written as

$$J_A = 2\mu A, \tag{24}$$

where A denotes the area of triangle in the (u, v) plane. Using the relationship

$$R - R_0 = \mu^m f(\mu, \beta) \tag{25}$$

and equation (23) in equation (22) leads to

$$I = \sum_j I_j = \sum_j \int_0^1 \int_0^1 \frac{g}{[\mu^m f(\mu, \beta) + R_0]^n} \, 2\mu A \, d\mu \, d\beta, \tag{26}$$

where j denotes the jth triangle. Herein, the value of m is set at two if the projection of the field point in the (γ, λ) co-ordinates is inside or on the boundary of the integration domain and set at one if the projection is outside the domain. Depending on the position of the field point relative to the panel, different forms of $f(\mu, \beta)$ in equation (26) can be derived so that the nearly singular kernel integral can be evaluated equally effectively in all practical cases. See Wu [19] for a detailed description of the function $f(\mu, \beta)$. Substituting the relationship

$$\alpha = \mu^m \tag{27}$$

into equation (26) yields

$$I = \sum_j I_j = \sum_j \int_0^1 \int_0^1 \frac{g}{[\alpha f(\alpha, \beta) + R_0]^n} \frac{2A\alpha^{2/m-1}}{m} \, \mathrm{d}\alpha \, \mathrm{d}\beta. \tag{28}$$

For convenience, consider a one-dimensional integral in the following form:

$$J = \int_0^1 \frac{h}{[\alpha f(\alpha) + R_0]^n} \, \mathrm{d}\alpha, \tag{29}$$

where h denotes a function. Equation (29) is a nearly singular integral for a small value of R_0. Applying a transformation formula

$$\alpha = \frac{1}{(c_1 + c_2\alpha^*)^l} - \delta, \tag{30}$$

in equation (29) leads to a regular integral

$$J = \int_{-1}^1 \frac{c_2 l h (c_1 + c_2\alpha^*)^{l(n-1)-1}}{[f(\alpha^*) + \delta(f(0) - f(\alpha^*)(c_1 + c_2\alpha^*)^l]^n} \, \mathrm{d}\alpha^*, \tag{31}$$

where $\delta = R_0/f(0, \beta)$. Equation (31) is regular because the function $f(\alpha^*)$ is always finite for $\alpha^* \in [-1, 1]$. The coefficients c_1 and c_2 are defined by

$$c_1 = \frac{(1+\delta)^{1/l} + \delta^{1/l}}{2\delta^{1/l}(1+\delta)^{1/l}}, \qquad c_2 = \frac{(1+\delta)^{1/l} - \delta^{1/l}}{2\delta^{1/l}(1+\delta)^{1/l}}, \tag{32}$$

where

$$l = \max\left[1, -\frac{\ln \delta}{\ln(2d)}\right], \quad d > \frac{1}{2\delta^{1/l}}. \tag{33}$$

In practice, the constant d is chosen to be as small as possible for the integration accuracy. Notably, equation (30) maps $\alpha(0, 1)$ to $\alpha^*(1, -1)$.

For illustration, consider the following integral:

$$I = \int_{-\pi/20}^{\pi/20} \int_{-1/40}^{1/40} \frac{1}{R^3} \, \mathrm{d}x \, \mathrm{d}y, \tag{34}$$

where $R = (x^2 + y^2 + z_0^2)^{1/2}$. Equation (34) represents an integral in a typical boundary element around the edge of a circular disk, which is a test case that will be presented in the next section. As Figure 1 illustrates, the sub-division method and the present method divide the integration domain into four and six sub-domains respectively. Correspondingly, total numbers of $4 \times N \times N$ quadrature points for the sub-division method and $6 \times M \times M$ points for the present method using the Gauss–Legendre formula are applied to evaluate equation (34). Note that each sub-domain of the present method has the same area, and the usage of four sub-domains for the sub-division method is only for computational convenience. The total number of quadrature points is known to be the main concern. Figure 2 plots the relative error, which is defined by |(calculated value–exact value)/exact value|, against

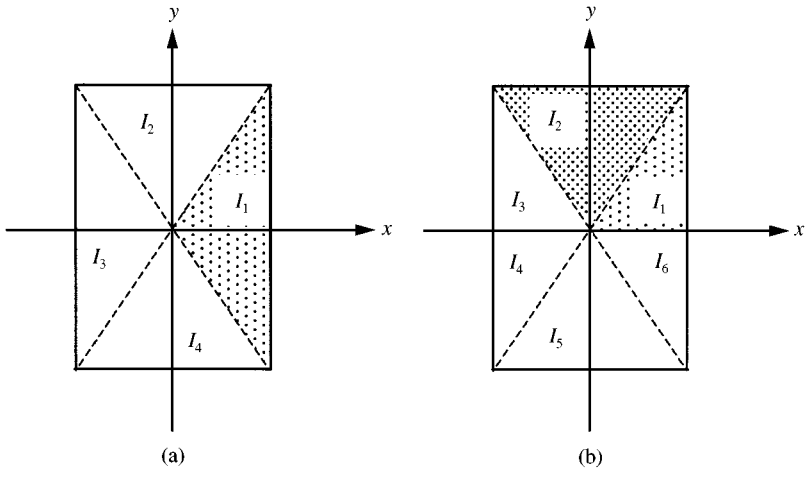

Figure 1. Sub-domains of integration for integral I in equation (34) using (a) the sub-division method and (b) the present method.

the total number of quadrature points for $z_0 = 0{\cdot}04$, $0{\cdot}01$. This figure indicates that the present method yields a greater accuracy than the sub-division method for both cases. According to Figure 2(b), the present method's efficiency is markedly improved for the smaller value of z_0. See Huang and Cruse [5] for a more detailed discussion on integration accuracy by varying the number of sub-elements and Gaussian points.

4. ILLUSTRATED EXAMPLES

A solution method is developed by combining the Helmholtz integral formulations in section 2 with the formulations in section 3. Under normal circumstances, the integral formulations in section 2 are used to remove the weak singularities and hypersingularity. The solution method also includes a simple, self-adaptive means of detecting the nearly singular kernels. Such a means determines when to use the formulae in section 3 to treat the nearly singular integrals. First, consider a circular cylinder with length $2h$ and radius a exposed to a plane wave incident in the direction of the negative z-axis (Figure 3). The edge effect is investigated by assigning $h/a = 1$. The coupling factor in Burton and Miller's method was set to be i/ka which is the best choice suggested by Burton [23] and Meyer *et al.* [24]. It is clear from physical considerations that this choice is to provide maximum absorption at the boundary; that is, the specific admittance should be unity. Herein, 20 collocation points along the θ direction and also along the r-direction yield 400 sub-surfaces on the lower and upper surfaces respectively. Twenty collocation points along the θ-direction and 40 points along the z-direction yield 800 sub-surfaces on the cylindrical surface. The order of quadrature formula in each element depends on the element's size. An absolute error of 10^{-5} for the integration along each element is generally prescribed. The LU decomposition method is used to solve the system of linear algebraic equations. Of particular concern in this problem are the characteristic wave numbers. The characteristic wave numbers for a circular cylinder are given by [25]

$$k_c a = \left[\left(\frac{n^* a \pi}{2h} \right)^2 + \alpha_{qs}^2 \right]^{1/2} \tag{35}$$

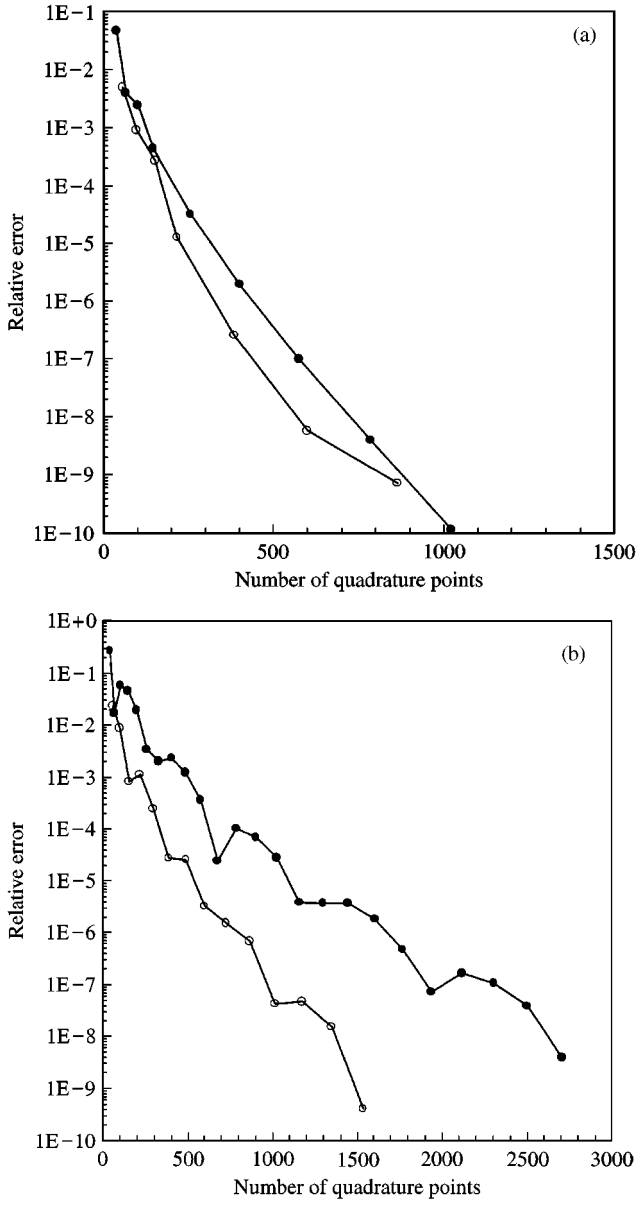

Figure 2. Relative error of integral I in equation (34) for (a) $z_0 = 0{\cdot}04$ and (b) $z_0 = 0{\cdot}01$ using the sub-division method (solid circle) and the present method (open circle).

in which n^* denotes a positive integer and α_{qs} denotes the sth root of the qth Bessel function, i.e.,

$$\mathbf{J}_q(\alpha_{qs}) = 0, \quad q = 0, 1, 2, \ldots \tag{36}$$

For $h/a = 1$, the first few characteristic wave numbers are 2·872, 3·956, 4·141, 4·955, 5·291, 5·370, 5·739, 6·020, 6·074, 6·351, 6·571, 6·728, 6·970, 7·112 and 7·189. Figure 4 displays the excess-pressure ratios $|p/p_0|$ on the upper and lower surfaces for the dimensionless wave

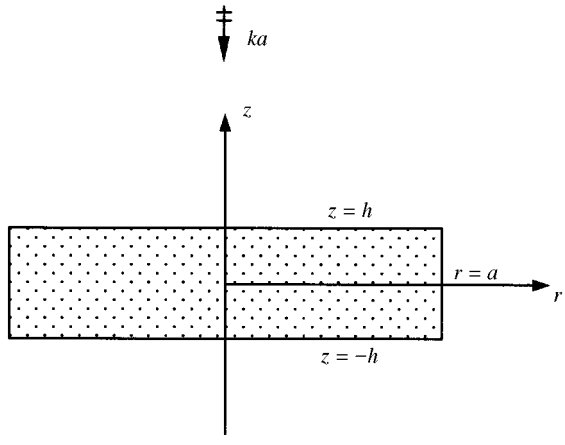

Figure 3. Co-ordinate system of a circular cylinder.

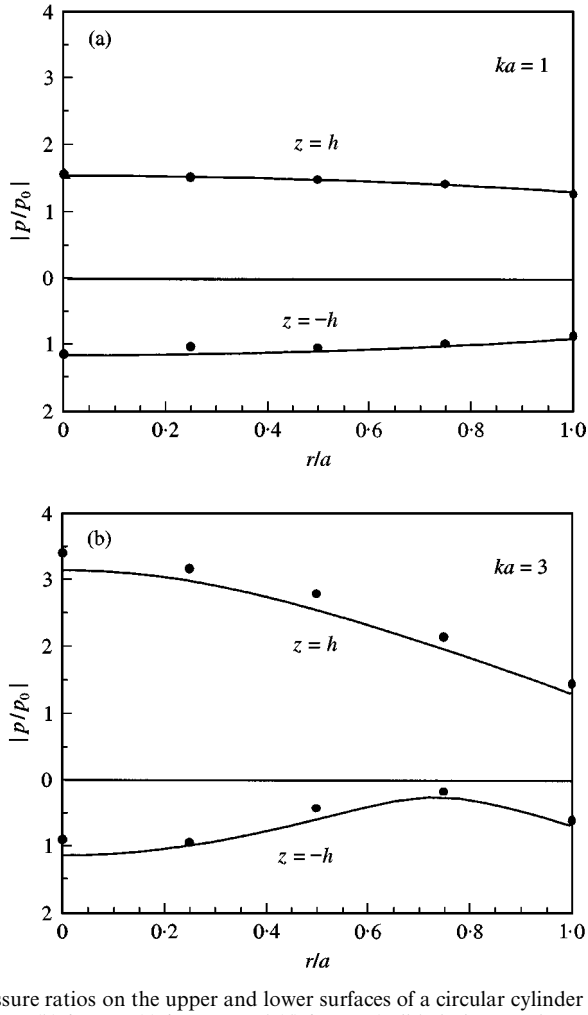

Figure 4. Excess-pressure ratios on the upper and lower surfaces of a circular cylinder with $h/a = 1$ exposed to a plane wave of (a) $ka = 1$, (b) $ka = 3$, (c) $ka = 5$, and (d) $ka = 7$ (solid circle: experimental results; solid line: the present numerical results).

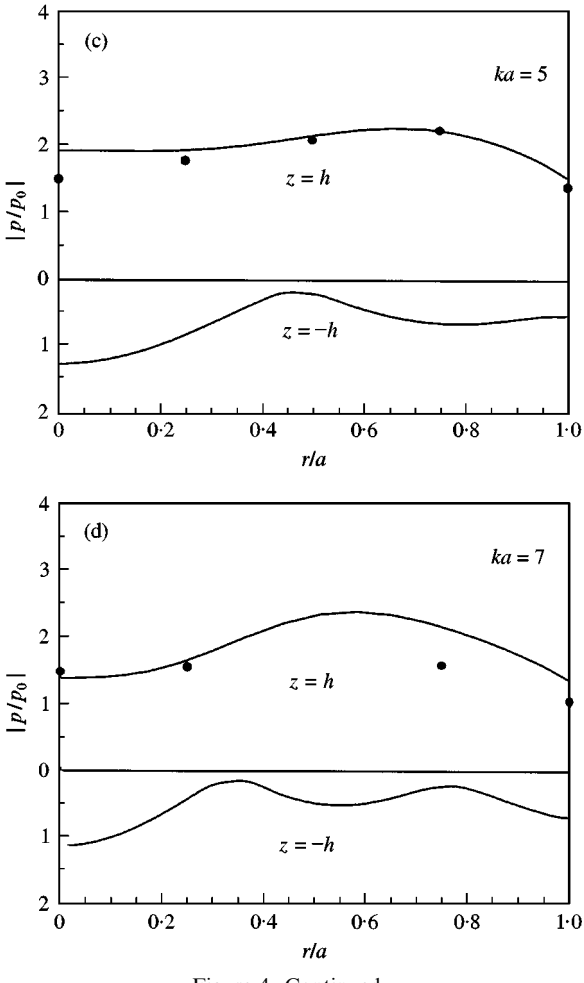

Figure 4. Continued.

number ka increasing from one to seven, where p_0 denotes the free-field pressure. Notably, the chosen values of ka are extremely close to the characteristic wave numbers with one exception, i.e., $ka = 1$. The proposed method's effectiveness is examined by comparing the calculated results with the experimental data [26]. For the lower ka's, the calculated results correlate well with the experimental data. For the higher ka's, i.e., $ka = 5$, 7, the computational accuracy is still acceptable since, under such circumstances, the experimental error in $|p/p_0|$ increases to around a value of one. This error is ascribed to an error in the frequency setting of the oscillator.

Next, consider two limiting cases, i.e., $h/a = 0{\cdot}0423$, $0{\cdot}02$, of the previous example. For $h/a = 0{\cdot}0423$, the first characteristic wave number appears at a value of $37{\cdot}212$. Although the first characteristic wave number markedly exceeds the chosen wave numbers, for convenience and preserving generality, the same solution method as in the previous example is applied for these two limiting cases. Owing to the small thickness, only one collocation point is applied along the z-direction and other distribution of collocation points resembles the previous example. Notably, every field point on the body surface contains both the singularity and near singularity. Figure 5 displays the excess-pressure

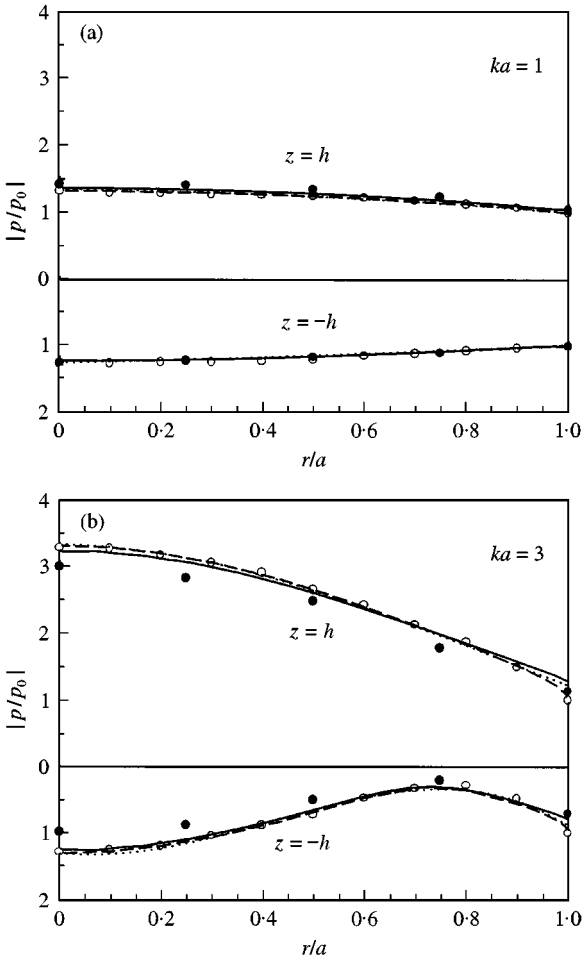

Figure 5. Excess-pressure ratios on the upper and lower surfaces of a circular disk exposed to a plane wave of (a) $ka = 1$, (b) $ka = 3$, (c) $ka = 5$, and (d) $ka = 7$ (solid circle: experimental results, $h/a = 0{\cdot}0423$; solid line: the present numerical results, $h/a = 0{\cdot}0423$; dotted line: the present numerical results, $h/a = 0{\cdot}02$; dashed line: the present analytical results, $h/a = 0$; open circle: Leitner's analytical results, $h/a = 0$).

ratios on the upper and lower surfaces for $h/a = 0{\cdot}0423$, $0{\cdot}02$ and ka increasing from one to seven. For comparison, this figure also plots the analytical solution for a circular disk with zero thickness. The analytical solution on the disk surface can be written as [27]

$$\phi^i + \phi^s = \frac{2}{c} \sum_{n=0}^{\infty} \frac{i^n}{\tilde{N}_{0n}} \frac{1}{R_{0n}^{(3)'}(-\mathrm{i}c, \mathrm{i}0)} S_{0n}(-\mathrm{i}c, -1) S_{0n}(-\mathrm{i}c, \eta), \tag{37}$$

where $c = ka$ and $\tilde{N}_{0n}$ is defined by the orthogonal relation

$$\int_{-1}^{1} S_{0n}(-\mathrm{i}c, \eta) S_{0n'}(-\mathrm{i}c, \eta)\, \mathrm{d}\eta = \delta_{0n'} \tilde{N}_{0n}, \quad \delta_{0n'} = \begin{cases} 0, & n' \neq n, \\ 1, & n' = n. \end{cases} \tag{38}$$

S_{0n} in equation (37) denotes the angular oblate spheroidal wave function of the first kind, and $R_{0n}^{(3)}$ is related to the radial oblate spheroidal wave functions of the first and

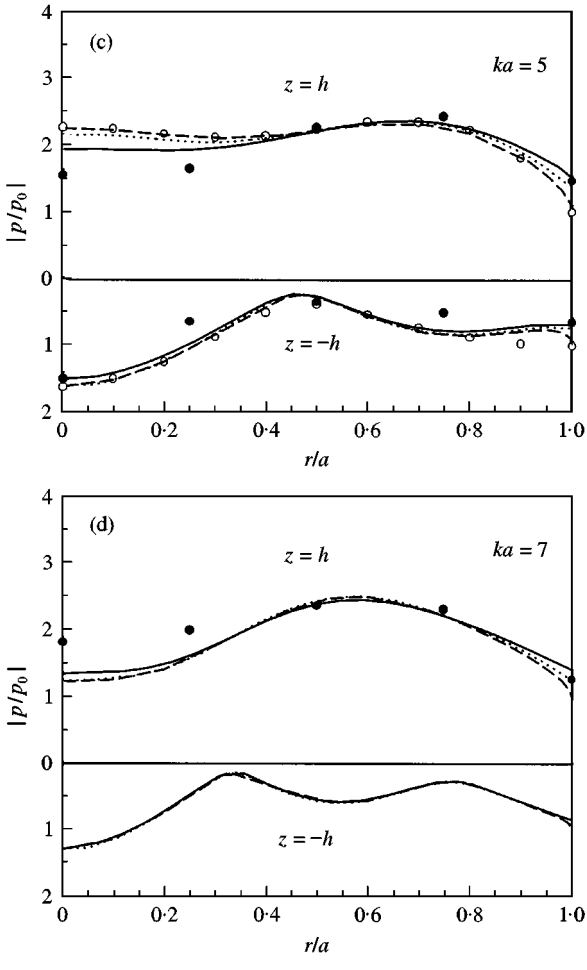

Figure 5. Continued.

second kinds by

$$R_{0n}^{(3)} = R_{0n}^{(1)} + \mathrm{i}R_{0n}^{(2)}. \tag{39}$$

In a related work, Leitner [28] presented the first numerical results of exact theory for the diffraction of sound by a circular disk up to $ka = 5$. Herein, we re-calculate the exact theory up to $ka = 7$. Figure 5 indicates that, in general, the proposed method's calculations for $h/a = 0{\cdot}0423$ correlate well with the experimental data. Equation (37) also yields satisfactory results with one exception, i.e., the region close to the edge. The discrepancy around the edge becomes more apparent with an increase in the wave number. This failure is ascribed to the fact that the value of a $|p/p_0|$ at $r/a = 1$ always remains one by applying the exact theory. This finding confirms the physical intuition that the thickness and edge effects of acoustic scattering by a disk-shaped body become more significant with an increase in the wave number, as also discussed by Wiener [26]. Figure 5 also depicts that the numerical results for $h/a = 0{\cdot}02$ and the zero-thickness solutions are closely correlated with one exception again, i.e., the region close to the edge. Therefore, under the circumstance of $h/a \leqslant 0{\cdot}02$ and low wave numbers, the proposed method and multidomain boundary

element method can function equally well to simulate the acoustic scattering by a disk-shaped body. The latter method is more attractive in numerical efficiency since no transformation (as presented in section 3) is necessary. However this method has problems in determining (1) the criterion in which the zero-thickness approximation is acceptable and (2) the tolerance limit in which the discrepancy due to the edge effect can be neglected. Notably, both the thickness and edge effects of a disk-shaped body are functions of the wave number, as mentioned earlier. Finally, also of notable concern is the difference between Leitner's and the present calculations using exact theory in the proximity of the edge of the shadow side for $ka = 5$ in Figure 5(c). This discrepancy may be attributed to the restricted ability of computing tools in Leitner's time.

5. CONCLUSIONS

This paper presents a solution method to investigate the acoustic scattering from rigid bodies with a focus on efficiently evaluating nearly singular integrals. The current method makes use of a composite integral equation which is free of weakly singular and hypersingular kernels, and a transformed integral which is free of weakly singular and hypersingular kernels, and a transformed integral which is free of nearly singular kernels. Comparing the numerical calculations with the available experimental data and analytical solutions confirms the effectiveness of the current method. According to the results, the current method outperforms the conventional sub-division method in terms of computational efficiency. Meanwhile, the current method avoids the zero-thickness limitation of the multidomain boundary element method. Therefore, the related edge and thickness effects can be investigated with accuracy and efficiency. These effects generally become more significant with an increase in the wave number. Under the circumstance of higher wave numbers, Yang's method [22] can be applied to assess the oscillatory integrals appearing in the integral formulation. A future study should incorporate an appropriate grid generation (local) method or a global method into the proposed method to resolve the related acoustical problems with generalized body shapes.

ACKNOWLEDGMENTS

The author would like to thank the National Science Council of the R.O.C. for partially supporting this research under contract no. NSC 87-2611-E-006-033 and Y. P. Lee for her programming assistance; S. Zhang and J. Jin allowing the author to use the subroutines contained in *Computation of Special Functions* (John Wiley & Sons, New York, 1996).

REFERENCES

1. H. A. SCHENCK 1968 *Journal of the Acoustical Society of America* **44**, 41–58. Improved integral formulation for acoustic radiation problems.
2. A. J. BURTON and G. F. MILLER 1971 *Proceedings of the Royal Society London. Series A* **323**, 201–210. The application of integral equation methods to the numerical solution of some exterior boundary value problems.
3. R. D. CISKOWSKI and C. A. BREBBIA (editors) 1991 *Boundary Element Methods in Acoustics*. Southampton: Computational Mechanics Publications, Chapters 1 and 3.
4. W. BENTHIEN and A. SCHENCK 1997 *Computers and Structures* **65**, 295–305. Nonexistence and nonuniqueness problems associated with integral equation methods in acoustics.
5. Q. HUANG and T. A. CRUSE 1993 *International Journal for Numerical Methods in Engineering* **36**, 2643–2659. Some notes on singular integral techniques in boundary element analysis.

6. C. J. HUANG, C. Y. CHEN and S. A. YANG 1998 *Proceedings of the National Science Council. R.O.C. Part A* **22**, 199–213. Diffraction of acoustic waves by perfectly soft bodies.
7. D. LEFEBER 1989 *Solving Problems with Singularities Using Boundary Elements*. Southampton: Computational Mechanics Publications, Chapter 1.
8. H. MOTZ 1946 *Quarterly of Applied Mathematics* **4**, 371–377. The treatment of singularities of partial differential equations by relaxation methods.
9. M. A. JASWON and G. T. SYMM 1977 *Integral Equation Methods in Potential Theory and Elastostatics*. London: Academic Press.
10. U. HEISE 1993 *Computational Mechanics* **12**, 1–18. Integral equations for the plane potential problem on domains with a corner or a slit.
11. V. SLADEK, J. SLADEK and M. TANAKA 1993 *International Journal for Numerical Methods in Engineering* **36**, 1609–1628. Regularization of hypersingular and nearly singular integrals in the potential theory and elasticity.
12. K. HAYAMI 1991 *Ph.D. thesis, Wessex Institute of Technology, Southampton*. A projection transformation method for nearly singular surface boundary element integrals.
13. W. HACKBUSCH and S. A. SAUTER 1992 *Computing* **52**, 139–159. On numerical cubatures of nearly singular surface integrals arising in BEM collocation.
14. K. HAYAMI and H. MATSUMOTO 1994 *Engineering Analysis with Boundary Elements* **13**, 143–154. A numerical quadrature for nearly singular boundary element integrals.
15. A. F. SEYBERT, C. Y. R. CHENG and T. W. WU 1990 *Journal of the Acoustical Society of America* **88**, 1612–1618. The solution of coupled interior/exterior acoustic problems using the boundary element method.
16. T. W. WU and G. C. WAN 1992 *Journal of the Acoustical Society of America* **92**, 2900–2906. Numerical modeling of acoustic radiation and scattering from thin bodies using a Cauchy principal integral equation.
17. G. KRISHNASAMY, F. J. RIZZO and Y. LIU 1994 *International Journal for Numerical Methods in Engineering* **37**, 107–121. Boundary integral equations for thin bodies.
18. W. S. HWANG 1997 *Journal of the Acoustical Society of America* **101**, 3336–3342. Hypersingular boundary integral equations for exterior acoustic problems.
19. S. WU 1995 *Communications in Numerical Methods in Engineering* **11**, 331–337. On the evaluation of nearly singular kernel integrals in boundary element analysis.
20. S. WU and P. A. LU 1996 *Communications in Numerical Methods in Engineering* **12**, 85–93. On the evaluation of nearly singular kernel integrals in boundary element analysis—some improved formulations.
21. S. A. YANG 1997 *Journal of the Acoustical Society of America* **105**, 93–105. On the singularity-free boundary integral equation formulation for two-dimensional acoustic scattering.
22. S. A. YANG 1997 *Journal of the Acoustical Society of America* **102**, 2511–2520. Acoustic scattering by a hard or soft body across a wide frequency range by the Helmholtz integral equation method.
23. A. J. BURTON 1976 *NPL Contract OC5*/535. Numerical solution of acoustic radiation problems.
24. W. L. MEYER, W. A. BELL, M. P. STALLYBRASS and B. T. ZINN 1979 *Journal of the Acoustical Society of America* **65**, 631–638. Prediction of the sound field radiated from axisymmetric surfaces.
25. J. VAN BLADEL 1964 *Electromagnetic Fields*, 308. New York: McGraw-Hill Book Co.
26. F. M. WIENER 1949 *Journal of the Acoustical Society of America* **21**, 334–347. The diffraction of sound by rigid disks and rigid square plates.
27. J. J. BOWMAN, T. B. A. SENIOR and P. L. E. USLENGHI (editors) 1987 *Electromagnetic and Acoustic Scattering by Simple Shapes*. New York: Hemisphere, Chapter 14.
28. A. LEITNER 1949 *Journal of the Acoustical Society of America* **21**, 331–334. Diffraction of sound by a circular disk.